JCIM JOURNAL OF CHEMICAL INFORMATION AND MODELING

Article

Cite This: J. Chem. Inf. Model. 2019, 59, 2913−2923

pubs.acs.org/jcim

Examining Product Specificity in Protein Arginine Methyltransferase 7 (PRMT7) Using Quantum and Molecular Mechanical Simulations

Abhishek Thakur,[‡] Joan M. Hevel,[†] and Orlando Acevedo*[,‡]

[‡]Department of Chemistry, University of Miami, Coral Gables, Florida 33146, United States

[†]Department of Chemistry and Biochemistry, Utah State University, Logan, Utah 84322, United States

Supporting Information

ABSTRACT: Protein arginine methyltransferase 7 (PRMT7) catalyzes the formation of monomethylarginine (MMA) but is incapable of performing a dimethylation. Given that PRMT7 performs vital functions in mammalian cells and has been implicated in a variety of diseases, including breast cancer and age-related obesity, elucidating the origin of its strict monomethylation activity is of considerable interest. Three active site residues, Glu172, Phe71, and Gln329, have been reported as particularly important for product specificity and enzymatic activity. To better understand their roles, mixed quantum and molecular mechanical (QM/MM) calculations coupled to molecular dynamics and free energy perturbation theory were carried out for the WT, F71I, and Q329S trypanosomal PRMT7 (TbPRMT7) enzymes bound with *S*-adenosyl-*L*-methionine (AdoMet) and an arginine substrate in an unmethylated or methylated form. The Q329S mutation, which experimentally abolished enzymatic activity, was appropriately computed to give an outsized $\Delta G^{\ddagger}$ of 30.1 kcal/mol for MMA formation compared to 16.9 kcal/mol for WT. The F71I mutation, which has been experimentally shown to convert the enzyme from a type III PRMT into a mixed type I/II capable of forming dimethylated arginine products, yielded a reasonable $\Delta G^{\ddagger}$ of 21.9 kcal/mol for the second turnover compared to 28.8 kcal/mol in the WT enzyme. Similar active site orientations for both WT and F71I TbPRMT7 allowed Glu172 and Gln329 to better orient the substrate for S_N2 methylation, enhanced the nucleophilicity of the attacking guanidino group by reducing positive charge, and facilitated the binding of the subsequent methylated products.

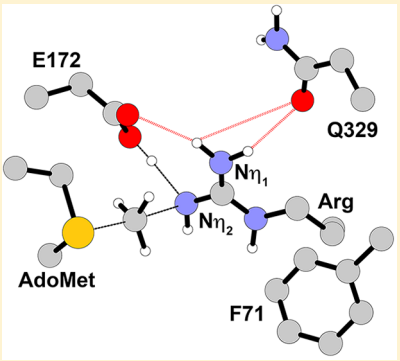

INTRODUCTION

Methylation of the guanidinium group in arginyl residues has significant implications in the regulation of signal transduction,[1,2] gene transcription,[3] RNA processing,[4] and other critical biological pathways.[5−10] Arginine methylation is widespread in mammals[11,12] and is primarily performed by a family of nine enzymes called protein arginine methyltransferases (PRMTs).[13,14] PRMTs catalyze the transfer of a methyl group from the cofactor *S*-adenosyl-*L*-methionine (AdoMet) to the guanidino nitrogen atoms of arginine in a substrate protein. This methyl group addition alters protein−protein interactions through steric effects, added hydrophobicity, and the disruption of hydrogen-bonding sites without a change in the cationic charge.[7,15] Three unique methylarginine products have been identified in animals: monomethylarginine (MMA), asymmetric dimethylarginine (ADMA), and symmetric dimethylarginine (SDMA). PRMTs are categorized into three different types according to their catalytic activity (Figure 1); type I (PRMT1, PRMT2, PRMT3, PRMT4/CARM1, PRMT6, and PRMT8) and type II (PRMT5 and PRMT9) form MMA prior to the formation of the dimethylated products ADMA and SDMA, respectively.[16] PRMT7 is a type III enzyme, unique in its ability to exclusively monomethylate substrates.[17]

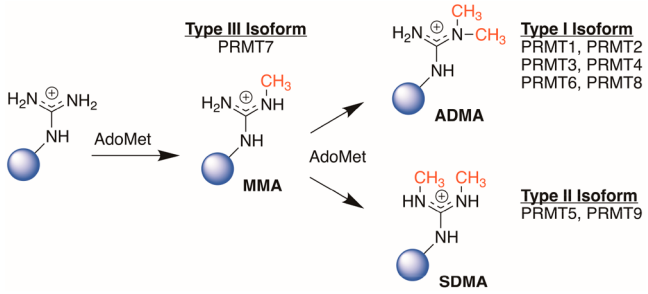

Figure 1. Methylation of arginyl residues catalyzed by three different types of PRMTs using *S*-adenosyl-*L*-methionine (AdoMet). PRMT7 is the only exclusive monomethyltransferase.

PRMT7 is one of the lesser characterized isoforms within the PRMT family despite performing important functions in mammalian cells that include the methylation of Sm-class ribonucleoproteins[18] and participating in DNA repair.[19] In addition, PRMT7 has been implicated in a variety of diseases, such as breast cancer,[20,21] age-related obesity,[22] DNA damage,[19] and SBIDDS (short stature, brachydactyly, intellectual developmental disability, and seizures) syndrome.[23]

Received: February 14, 2019
Published: April 29, 2019

DOI: 10.1021/acs.jcim.9b00137
J. Chem. Inf. Model. 2019, 59, 2913−2923

An initial misclassification of PRMT7 as a type II PRMT (capable of producing both MMA and SDMA), possibly a consequence of PRMT5 contamination due to purification methods,[13,14] complicated earlier analyses of product specificity.[19,24] Subsequent studies have confirmed PRMT7 to be a type III PRMT enzyme, i.e., capable only of MMA production;[25−29] however, the origin of its unique product specificity compared to the other natural isoforms remains unclear. Part of the difficulty in studying the system comes from the weak activity observed in the human PRMT7.[25,26] An alternative homologue, TbPRMT7, from *Trypanosoma brucei*, a parasitic protozoan responsible for spreading African sleeping sickness, exhibits the highest sequence identity to human PRMT7 and possesses significant *in vitro* activity toward multiple substrates.[28] Interestingly, TbPRMT7 is expressed as a single polypeptide containing a single active site compared to the human PRMT7 which expresses as a single polypeptide housing two active sites with a unique nonfunctional C-terminal domain.[25]

Reported crystal structures of different orthologs of PRMT7 have identified a considerably narrow binding pocket, suggesting that the small volume may impede the formation of a dimethylated product due to unfavorable steric effects.[30−32] Interestingly, site-directed mutagenesis studies on TbPRMT7 have reported that the Glu181Asp and Gln329Ala mutants are capable of producing SDMA, perhaps a consequence of an increased volume size in the active site.[31,32] However, Gln329 is a bulky histidine residue in PRMT1 and Glu181 is conserved between all PRMT types (i.e., I, II, and III), which highlights the subtle complexities in trying to unravel PRMT7's product specificity. Our own joint experimental and computational study identified Phe71 as a key residue for dictating MMA formation in TbPRMT7. In PRMT1, which can make ADMA, this residue is an isoleucine. Interestingly, the Phe71Ile variant was able to produce all three different arginine products, i.e., MMA, ADMA, and SDMA.[33] Mutation of the same residue to a serine (Phe71Ser), corresponding to the sequence in human PRMT7, produced solely the MMA product in TbPRMT7. In addition, a Phe71Ala TbPRMT7 mutant also exclusively yielded MMA, calling into question a direct connection between overall volume size in the active site and product specificity. Molecular dynamics simulations found that only the Phe71Ile mutation maintained the proper geometry within the active site for optimal S_N2 methyl transfer.[33] However, a detailed mechanistic study that incorporates electronic effects into the calculation is lacking, but crucial for understanding the role that specific residues play in product specificity.

Mixed quantum and molecular mechanical (QM/MM) calculations coupled to molecular dynamics sampling and utilizing potentials of mean force simulations (MD/PMF) were carried out here to elucidate the origin of the MMA product exclusivity in WT TbPRMT7. The enzymatic system was bound with AdoMet and a (1) ASGRG substrate or (2) a monomethylated ASGRG substrate where the methyl group is either covalently bound to the $N_{\eta 1}$ nitrogen (MMA-$N_{\eta 1}$) or the $N_{\eta 2}$ nitrogen (MMA-$N_{\eta 2}$), as defined in Figure 2. In addition, the F71I TbPRMT7 mutant, which is capable of forming all three arginine products, and the Q329S TbPRMT7 mutant was studied using the QM/MM MD/PMF methodology. This study further clarifies how the active site residues Glu172, Glu181, Phe71, and Gln329 within PRMT7 impact both product specificity and enzymatic activity.

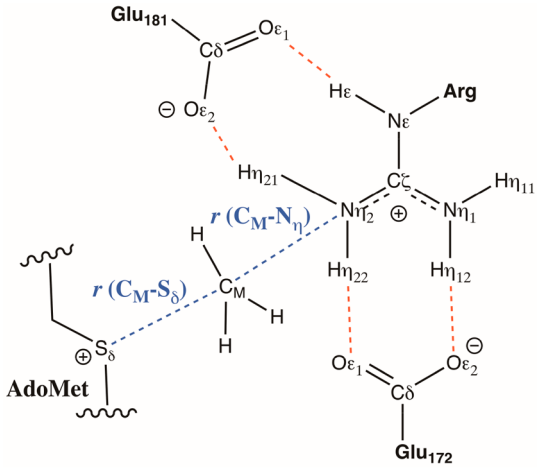

Figure 2. In the QM/MM/MD calculations, the QM region encompassed the unmethylated or methylated arginine substrate, AdoMet, and Glu172 or Glu181. The PMF reaction coordinate for the methyl transfer is $\{r(C_M{-}S_\delta) - r(C_M{-}N_\eta)\}$, where $\{r(C_M{-}S_\delta) + r(C_M{-}N_\eta)\} = 4.4$ Å.

METHODS

Computational Enzyme Preparation. Simulation of the *Trypanosoma brucei* PRMT7 required the generation of initial Cartesian coordinates derived from a 2.04 Å resolution crystal structure (PDB ID: 4M38).[30] A monomer was simulated containing the amino acids 41−374, as the N-terminal region lacked clear electron density. The cocrystallized AdoHcy was methylated to form (*S*,*S*)-AdoMet. In our solved TbPRMT7 crystal structure, the electron density of the first four residues of the $H4^{1\text{-}21}$ peptide substrate (SGRG) was observed.[30] An alanine residue was added to the SGRG substrate (ASGRG) in a similar fashion to our previous MD simulation of TbPRMT7.[33] Mutations to TbPRMT7 active site residues were made using the Yasara software.[34] Hydrogen atoms were added using the tleap module in the AMBER software.[35] Details of equilibration of the WT and mutant enzymes prior to QM/MM calculations are provided below.

MD Protocol. Molecular dynamics (MD) simulations were performed on different enzyme/substrate complexes for the WT and mutant TbPRMT7 systems. Explicit solvent was utilized with an orthorhombic TIP3P water box[36] that extended at least 10 Å beyond the enzyme. Charge neutrality was maintained by adding an appropriate number of sodium ions. The ff14SB force field[37] was employed in the construction of the topology files for the protein and peptide substrate, whereas the AdoMet parameters were provided from the generalized AMBER force field (GAFF).[38] The water molecules and Na^+ ions in the initial structures were conjugate gradient (CG) minimized for 2000 steps, followed by 10,000 steps of CG optimization for the entire system. Following minimization, the full system was slowly heated from 0 to 300 K over 50 ps of MD with a constant NVT ensemble that used the weak-coupling algorithm and a temperature coupling value of 2.8 ps. To correct the density, the system was switched to a constant NPT ensemble and ran for 500 ps at 300 K and 1 atm using a coupling value of 2.0 ps for both temperature and pressure. Following equilibration, unbiased MD production data was collected for 100 ns at constant NVT for each protein complex using the GPU-accelerated version of AMBER 16.[39] Long-range electrostatics were accounted for by using the

DOI: 10.1021/acs.jcim.9b00137
J. Chem. Inf. Model. 2019, 59, 2913−2923

Table 1. Computed Free Energies of Activation, $\Delta G^{\ddagger}$, and Reaction, ΔG_{rxn}, (kcal/mol), for the First Methyl Transfer from AdoMet to the $N_{\eta 1}$ and $N_{\eta 2}$ Atoms of the Naked Arginine Peptide in the WT, F71I, and Q329S TbPRMT7 Enzymes To Yield MMA-$N_{\eta 1}$ and MMA-$N_{\eta 2}$, Respectively

base	PRMT7	$\Delta G^{\ddagger}$ MMA-$N_{\eta 1}$	$\Delta G^{\ddagger}$ MMA-$N_{\eta 2}$	ΔG_{rxn} MMA-$N_{\eta 1}$	ΔG_{rxn} MMA-$N_{\eta 2}$
E181	WT	N/A[a]	47.3 ± 0.2	N/A[a]	39.5 ± 0.5
E172	WT	21.3 ± 1.1	16.9 ± 0.1	−15.3 ± 1.3	−20.9 ± 0.3
E172	F71I	32.5 ± 1.5	18.3 ± 0.7	−8.7 ± 1.7	−16.0 ± 0.1
E172	Q329S	N/A[a]	30.1 ± 1.4	N/A[a]	−9.6 ± 0.9

[a]Did not energetically converge.

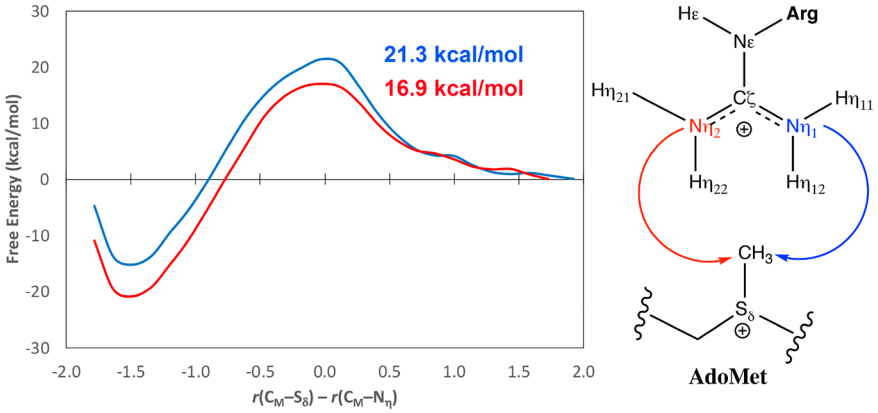

Figure 3. Free energy profiles and $\Delta G^{\ddagger}$ for the methyl transfer from AdoMet to the $N_{\eta 1}$ atom (blue) and $N_{\eta 2}$ atom (red) of the unmethylated arginine peptide using E172 as the active site base in WT TbPRMT7.

particle mesh Ewald, all covalent bonds involving hydrogen atoms were constrained with the SHAKE algorithm, periodic boundary conditions were enforce using a nonbonded cutoff distance of 12 Å, and a time step of 1.0 fs was employed.

QM/MM/MD Calculations. Mixed quantum mechanics and molecular mechanics (QM/MM) calculations[40,41] employing molecular dynamics sampling were performed on the WT and mutant TbPRMT7 systems. The QM region encompassed the unmethylated or methylated arginine substrate, AdoMet, and Glu172 or Glu181 and were treated using the self-consistent charge density functional tight-binding (SCC-DFTB) semiempirical method[42] as implemented in the AMBER package.[43] Additional SCC-DFTB parameters were included into AMBER using the DFTB+ 1.2.2 software.[44] A previous QM/MM/MD study on PRMT3 found that SCC-DFTB gave energetics similar to B3LYP/6-31G(d,p).[45] Multiple reviews have reported the SCC-DFTB methodology to be quite accurate and comparable to other semiempirical, e.g., PDDG/PM3,[46] and *ab initio* methods for many wide-ranging QM/MM-based enzymology studies.[47−49] The remainder of the protein utilized the ff14SB force field.[37] The interactions of overlapped atoms in the QM and MM regions were described through a "link atom" approach in AMBER,[50] which used hydrogen atoms in the QM region that overlapped the C_{α} atom position for the amino acid residues in the MM region. The AdoMet cofactor was truncated to the $-CH_2-CH_2-S^+(Me)-CH_2-$ portion in the QM region with a link atom located on each end. The enzyme was solvated using a periodic TIP3P water box, similar to the unbiased MD simulations described previously. The water molecules and Na^+ ions in the initial structures were CG minimized for 2000 steps, followed by 10 000 steps of CG optimization for the entire system.

Umbrella sampling[51] and the weighted histogram analysis method (WHAM)[52] was used to determine the changes in free energy, i.e., potentials of mean force (PMF),[40,41,53] for the methyl transfer from AdoMet to the arginine substrate to yield one of three unique methylarginine products: MMA, ADMA, or SDMA. The distance between the S atom of AdoMet and N atom ($N_{\eta 1}$ or $N_{\eta 2}$) of arginine was fixed to a distance of $\{r(C_M-S_{\delta}) + r(C_M-N_{\eta})\} = 4.4$ Å by employing a force constant of 1400 kcal mol^{-1} $Å^{-1}$ in the harmonic biasing potentials used in the 1D free energy simulations. A linear combination of the distances $\{r(C_M-S_{\delta}) - r(C_M-N_{\eta})\}$ was applied as the reaction coordinate for the 1-D PMF calculations (Figure 2). Multiple PMF windows, ca. 25−45, featuring 0.04−0.1 Å distance increments and a harmonic biasing potential force constant value of 400 kcal mol^{-1} $Å^{-1}$ were utilized to construct each potential energy surface. The systems were gradually heated from 0 to 310 K in 50 ps and then equilibrated for 50 ps using an NPT ensemble. For each FEP window, an additional 50 ps of equilibration was performed followed by a 50−70 ps QM/MM/MD production run in the NPT ensemble. A 1 fs time step for integration was used in all simulations. Error bars for the free energies were estimated by splitting the last 50 ps from each trajectory into three equal time points of 16.7 ps and computing the standard deviations in a similar fashion to previous QM/MM/MD studies.[54,55]

RESULTS AND DISCUSSION

WT TbPRMT7. To study the origin of product specificity in PRMT7 from an energetic perspective, mixed quantum and molecular mechanical calculations in conjunction with molecular dynamics sampling (QM/MM/MD) were carried out on the WT system by placing AdoMet, the naked or methylated arginine peptide, and an active site base in the QM

DOI: 10.1021/acs.jcim.9b00137
J. Chem. Inf. Model. 2019, 59, 2913−2923

region with the remainder of the protein, solvent, and counterions treated in the MM region. Potentials of mean force (PMF) calculations provided potential free energy surfaces from which free energies of activation ($\Delta G^{\ddagger}$) and free energies of reaction (ΔG_{rxn}) could be derived. Two invariant glutamate residues from the "double-E" hairpin loop are structurally conserved among PRMT family members, e.g., Glu144 and Glu153 in PRMT1,[56] and are required for enzymatic activity. In the case of TbPRMT7 these correspond to carboxylate side chains of Glu172 and Glu181. Our molecular dynamics simulations found significant hydrogen bonding occurred between Glu172 and the arginine of the peptide substrate, with a very high percent occupancy of 93−98% over the course of the simulation for WT TbPRMT7.[33] A smaller hydrogen bonding percent occupancy of 52−60% between Glu181-Arg in WT TbPRMT7 was also computed, which suggested a preference for Glu172 as the active site base. Accordingly, the present QM/MM/MD calculations found Glu181 gave an outsized $\Delta G^{\ddagger}$ of 47.3 ± 0.2 kcal/mol when performing the role of the active site base compared to 16.9−21.3 kcal/mol for Glu172 (Table 1).

During the S_N2 reaction mechanism, either guanidino nitrogen atom ($N_{\eta 1}$ or $N_{\eta 2}$ as defined in Figure 2) from Arg could potentially function as the nucleophile. The present QM/MM/MD calculations predicted a lower $\Delta G^{\ddagger}$ of 16.9 ± 0.1 kcal/mol for the $N_{\eta 2}$ position compared to 21.3 ± 1.1 kcal/mol for the $N_{\eta 1}$ position in the WT TbPRMT7 enzyme (Figure 3). The simulations also predicted a lower free energy of reaction, ΔG_{rxn}, for the monomethylated product in the MMA-$N_{\eta 2}$ orientation with a value of −20.9 ± 0.3 kcal/mol compared to −15.3 ± 1.3 kcal/mol for the MMA-$N_{\eta 1}$ conformation (Table 1 and Supporting Information Figure S1). The potential energy surfaces were reasonably similar to prior QM/MM/MD simulations of PRMT3, where the transfer of methyl from AdoMet to the $N_{\eta 1}$ or $N_{\eta 2}$ atoms of Arg gave $\Delta G^{\ddagger}$ values of 28.5 and 20.4 kcal/mol, respectively.[45] In addition, QM/MM/MD calculations of PRMT5 yielded $\Delta G^{\ddagger}$ values of 20.4 and 29.4 kcal/mol for $N_{\eta 1}$ and $N_{\eta 2}$, respectively.[57]

The favored S_N2 mechanism from the QM/MM/MD calculations, i.e., resulting in the MMA-$N_{\eta 2}$ binding orientation, gave symmetrical $r(C_M{-}S_\delta)$ and $r(C_M{-}N_{\eta 2})$ transition state distances of 2.2 ± 0.06 and 2.2 ± 0.04 Å, respectively. The average structure for the WT PRMT7 complex from the transition state free energy perturbation (FEP) window is shown in Figure 4. While this MMA-$N_{\eta 2}$ formation pathway gave average transition state distances of 1.1 ± 0.1 and 1.7 ± 0.3 Å for the proton transfer between the $N_{\eta 2}$ and $O_{\varepsilon 1}$ atoms, i.e., $O_{\varepsilon 1}\cdots H_{\eta 22}\cdots N_{\eta 2}$, the actual proton movement between the heteroatoms occurred almost instantaneously at the PMF window involving the transition state. Close distances of 2.4 ± 0.2 and 2.0 ± 0.2 Å at the transition state and reactants, respectively, between the Glu172 $O_{\varepsilon 2}$ atom and $H_{\eta 12}{-}N_{\eta 1}$, the hydrogen atom on the opposite guanidino nitrogen atom, are indicative of sustained hydrogen bonding over the course of the reaction (Figure 4B). Consequently, in addition to acting as the active site base, the Glu172 residue helped to anchor and orient the peptide substrate in the active site for S_N2 attack. The arginine substrate is better positioned for S_N2 attack with AdoMet when yielding MMA-$N_{\eta 2}$ as compared to MMA-$N_{\eta 1}$ (Supporting Information Figure S2). The Phe174 residue backbone oxygen atom and Glu172 carboxylate group

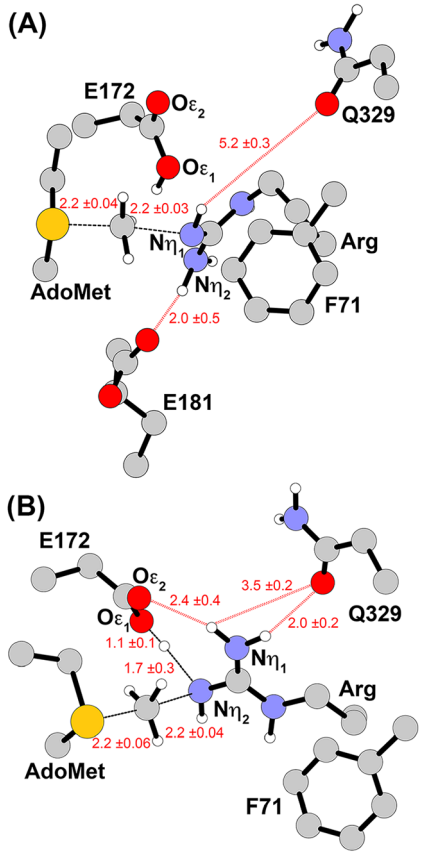

Figure 4. Active site structure from the QM/MM/MD transition state FEP window for the first methyl transfer from AdoMet to the (A) $N_{\eta 1}$ atom and (B) $N_{\eta 2}$ atom of the arginine peptide in WT TbPRMT7. Distances in angstroms.

also provided hydrogen bonding to the guanidino group thereby reducing positive charge during the reaction.

The Gln329 residue located on the THW loop has been shown to play a major role in product specificity.[32] The importance of this residue is further cemented as Q329S and Q329H experimental mutations completely deleted or largely decreased the activity of TbPRMT7.[30] The present QM/MM/MD calculations reproduced the site-directed mutagenesis experiments as the Q329S TbPRMT7 mutant gave a large $\Delta G^{\ddagger}$ of 30.1 ± 1.4 kcal/mol in the MMA-$N_{\eta 2}$ orientation and did not energetically converge for MMA-$N_{\eta 1}$ (Table 1). Molecular dynamics simulations reported a hydrogen bond percent occupancy of 77.8% between Gln329 and the arginine substrate over the course of the simulation for WT TbPRMT7.[33] The close distances of 2.0 ± 0.2 and 1.9 ± 0.2 Å computed for Q329-O$\cdots H_{\eta 11}{-}N_{\eta 1}$ at both the transition state and reactant regions of WT TbPRMT7, respectively, underscore the significance of this intermolecular interaction throughout the entire MMA-$N_{\eta}2$ reaction pathway (Figure 4B). The alternative nucleophilic attack from the opposite guanidino $N_{\eta 1}$ atom to yield the MMA-$N_{\eta 1}$ product also followed an S_N2 mechanism with similar $r(C_M{-}S_\delta)$ and $r(C_M{-}N_{\eta 1})$ distances compared to the MMA-$N_{\eta 2}$ configuration. However, in this case the Gln329 residue moved away from the substrate to a 5.2 ± 0.3 Å distance at the transition state, significantly reducing electrostatic stabilization of the guanidino moiety (Figure 4A). Accordingly, generalized Born (GB) free energy decomposition calculations[58] performed here with

DOI: 10.1021/acs.jcim.9b00137
J. Chem. Inf. Model. 2019, 59, 2913−2923

AdoMet bound in the active site found a large substrate binding free energy (ΔG_{bind}) contribution from Gln329 for the MMA-$N_{\eta 2}$ orientation with a value of -2.7 ± 0.7 kcal/mol compared to the negligible -0.1 ± 0.3 kcal/mol for the MMA-$N_{\eta 1}$ configuration (Supporting Information Table S1). Overall, the QM/MM/MD calculations emphasized that Glu172 and Gln329 in WT TbPRMT7 are key residues for properly orienting the peptide during the first S_N2 directed methylation. Additional hydrogen bonding contributions were provided by Phe174 and Thr176 to reduce the positive charge on the arginine during the transition state (Supporting Information Figure S2).

The sequential transfer of methyl groups onto a single arginine peptide can proceed in either a processive manner, i.e., does not release the substrate prior to the second methylation, or in a distributive manner, where the substrate is released after the first methylation to give MMA as the predominant product.[59−63] Kinetic analyses of PRMTs have yielded conflicting results of the processivity.[60,62,64,65] Assuming a processive mechanism for PRMT7,[66] QM/MM/MD suggests the second methyl transfer would occur on the MMA-$N_{\eta 2}$ orientation as the first turnover leading to that binding configuration possessed lower $\Delta G^{\ddagger}$ and ΔG_{rxn} values compared to the MMA-$N_{\eta 1}$ conformation (Figure 3). After rebinding AdoMet, the QM/MM/MD simulation gave a $\Delta G^{\ddagger}$ of 28.8 ± 0.3 kcal/mol for the second methyl addition to MMA-$N_{\eta 2}$ that yielded the ADMA-$N_{\eta 2}$ dimethylation product (Table 2).

Table 2. Computed Free Energies of Activation ($\Delta G^{\ddagger}$; kcal/mol) for the Second Methyl Transfer from AdoMet to the $N_{\eta 1}$ and $N_{\eta 2}$ Atoms of the MMA Peptide in the WT and F71I TbPRMT7 Enzymes to yield ADMA or SDMA

PRMT7	ADMA-$N_{\eta 1}$[a]	SDMA-$N_{\eta 1}$[a]	ADMA-$N_{\eta 2}$[b]	SDMA-$N_{\eta 2}$[b]
WT	29.9 ± 0.2	22.7 ± 0.7	28.8 ± 0.3	N/A[c]
F71I	N/A[c]	N/A[c]	21.9 ± 0.7	30.5 ± 1.2

[a]MMA bound in conformation where methyl group was covalently bonded at the $N_{\eta 1}$ position prior to reaction (i.e., MMA-$N_{\eta 1}$). [b]MMA bound in conformation where methyl group was covalently bonded at the $N_{\eta 2}$ position prior to reaction (i.e., MMA-$N_{\eta 2}$). [c]Did not energetically converge.

Calculations for the SDMA-$N_{\eta 2}$ reaction pathway did not energetically converge, which is indicative of poor steric interactions within the active site. The larger activation barrier for the ADMA formation relative to monomethylation is consistent with the experimental absence of dimethylated products in WT PRMT7. Examining the average transition structure leading to the formation of ADMA (Figure 5) found that many of the interacting distances between the Glu172 and Gln329 residues and the MMA substrate were relatively similar to those of the addition of the first methyl group to the $N_{\eta 2}$ atom of the naked arginine peptide (Figure 4B). However, binding both MMA-$N_{\eta 2}$ and AdoMet into WT TbPRMT7 reorganized the active site such that the E172-$O_{\varepsilon 2}$ atom no longer hydrogen bonded with the $H_{\eta 12}-N_{\eta 1}$ atom reducing the residue's ability to anchor the methylated substrate within the active site (Supporting Information Figure S3). In addition, the reacting distance between AdoMet and the arginine, $r(C_M-S_\delta)$, had a larger error bar of 2.1 ± 0.2 Å (Figure 5), suggesting significant movement occurring in the active site during the transition state window; for comparison, the naked peptide had a value of 2.2 ± 0.06 Å (Figure 4B).

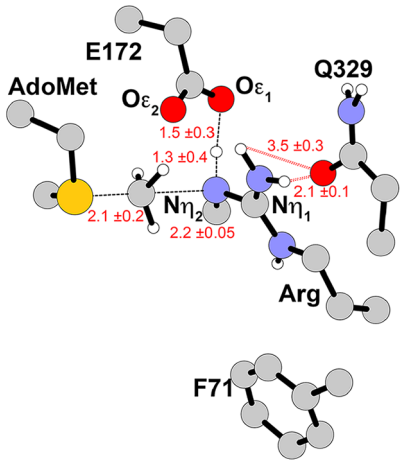

Figure 5. Active site structure from the QM/MM/MD transition state FEP window for the second methyl transfer from AdoMet to give ADMA product for the MMA-$N_{\eta 2}$ peptide conformation in WT TbPRMT7. Distances are in angstroms.

If the enzyme followed a distributive mechanism instead, the MMA product would dissociate from PRMT7 after the initial methylation. For a second turnover to occur, the monomethylated substrate would need to re-enter the PRMT7 enzyme along with an AdoMet cofactor through a relatively narrow entrance into the arginine binding pocket.[66] Rebinding the substrate in the thermodynamically favored MMA-$N_{\eta 2}$ orientation as before would yield the large $\Delta G^{\ddagger}$ of 28.8 ± 0.3 kcal/mol that would again impede ADMA-$N_{\eta 2}$ formation. Supposing the substrate bound in the less energetically favorable MMA-$N_{\eta 1}$ conformation, the QM/MM/MD calculations predicted a similar $\Delta G^{\ddagger}$ of 29.9 ± 0.2 kcal/mol when leading to the ADMA-$N_{\eta 1}$ product (Figure 6 and Table 2). Intriguingly, the alternative reaction yielding SDMA-$N_{\eta 1}$ gave a significantly lower $\Delta G^{\ddagger}$ of 22.7 ± 0.7 kcal/mol. In this case, the activation barrier was approximately 5 kcal/mol larger than the initial methylation of the naked peptide. While the reaction distances for AdoMet and the arginine residue were nearly identical between the methylated and naked substrate at the transition state, i.e., $r(C_M-S_\delta)$ and $r(C_M-N_{\eta 2})$ = 2.2, the Gln329 residue moved away from the substrate to a distance of 4.5 ± 0.2 Å to better accommodate the MMA-$N_{\eta 1}$ orientation within the active site (Figure 7). The preference for SDMA formation in the MMA-$N_{\eta 1}$ conformation appeared to correlate with greater hydrogen bonding between the Glu172 oxygen atoms and the $H_{\eta 12}$ and $H_{\eta 22}$ arginine atoms (Supporting Information Figure S4). For example, SDMA formation featured Glu172−Arg distances nearly identical to that of monomethylation, e.g., 2.4 Å for E172-$O_{\varepsilon 2}\cdots H_{\eta 12}$-Arg, see Figures 7B and 4B. Whereas, ADMA formation had the Glu172 side chain pointing away from the arginine substrate with a large distance of 3.0 ± 0.3 Å from the arginyl $H_{\eta 12}$ atom suggesting the deprotonation had occurred prior to the methyl transfer (Figures 7A and S4).

The size of two distinct subregions within the active site has been suggested to play a major role in PRMT7 product specificity.[32] Accordingly, the volume of the PRMT7 active site was monitored over the course of the simulation for the second methylation transition states in the MMA-$N_{\eta 1}$ and MMA-$N_{\eta 2}$ conformations. The size was determined using the POVME program[67] by selecting an amino acid near the center of the

DOI: 10.1021/acs.jcim.9b00137
J. Chem. Inf. Model. 2019, 59, 2913−2923

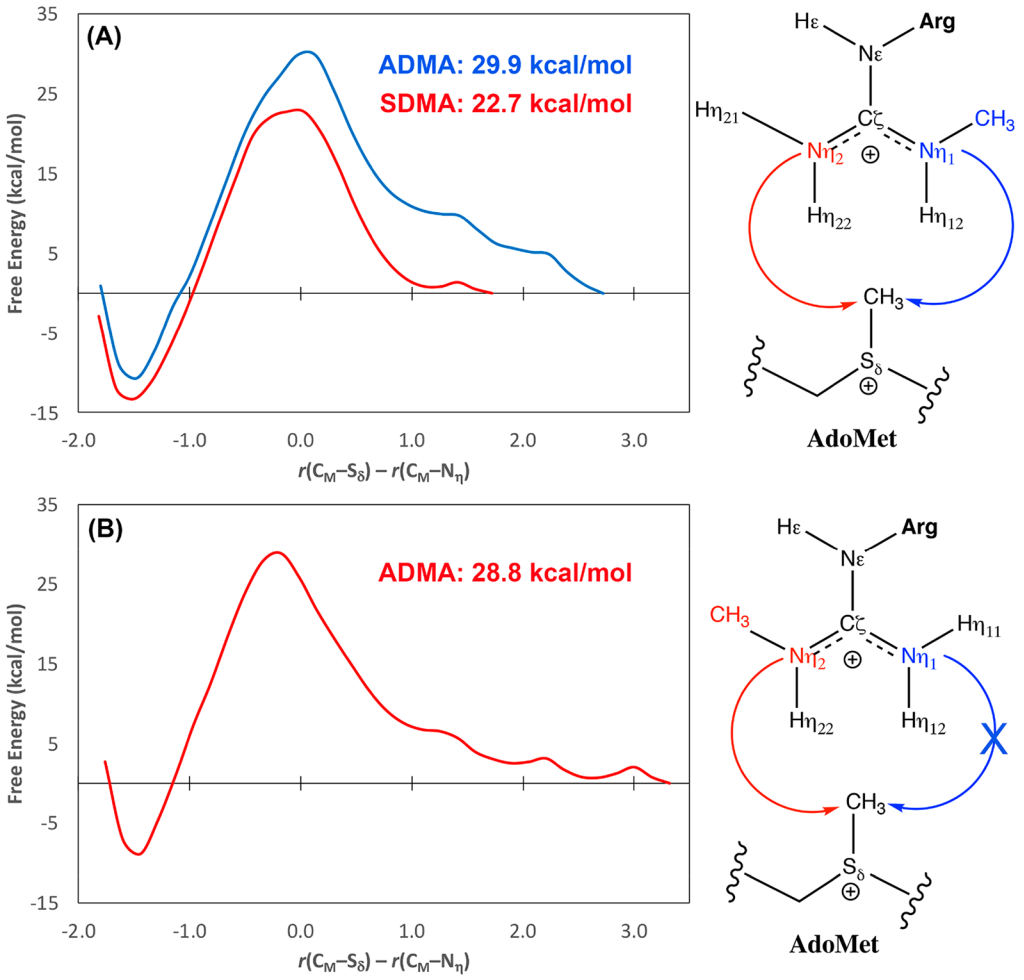

Figure 6. Free energy profiles and $\Delta G^{\ddagger}$ for the second methyl transfer from AdoMet to the $N_{\eta 1}$ atom (blue) and $N_{\eta 2}$ atom (red) of the MMA-$N_{\eta 1}$ (top) and MMA-$N_{\eta 2}$ (bottom) bound peptides in WT TbPRMT7.

active site, Trp330 in this case, and generating an inclusion sphere with a grid spacing of 1.0 Å and radius of 9.0 Å. The system with the lowest computed activation barrier, i.e., the formation of SDMA-$N_{\eta 1}$, possessed the smallest active site volume of 9 $Å^3$ compared to 18 and 19 $Å^3$ for ADMA-$N_{\eta 1}$ and ADMA-$N_{\eta 2}$ formation, respectively. It was rationalized that a more spacious binding pocket may enable dimethylation; for example, the SDMA-producing Glu181Asp/Gln329Ala TbPRMT7 double variant and the ADMA-producing Glu181Asp TbPRMT7 mutant both had higher binding affinities toward the monomethylated histone $H4^{1-21}$ R3MMA peptide than the unmethylated peptide.[31,32] However, the current calculations suggest that a larger active site volume alone does not aid in the formation of a dimethylation product as the ADMA binding orientation had a significantly larger volume than SDMA but gave larger $\Delta G^{\ddagger}$ values of 28.8–29.9 kcal/mol compared to 22.7 kcal/mol, respectively (Table 2). Instead, in a similar fashion to the naked peptide, favorable intermolecular interactions between the arginine substrate and the active site residues Glu172 and Gln329 appear to be largely responsible for both orienting and stabilizing the transition structure during the second methylation reaction (Supporting Information Figure S4).

F71I TbPRMT7. Our previous study of TbPRMT7 identified Phe71 as a key residue for dictating product specificity.[33] The mutation of Phe71 to Ile converted the enzyme from a type III PRMT into a mixed type I/II capable of forming three different arginine products (MMA, ADMA, and SDMA). Our calculations found that changing residue size at position 71, e.g., larger residues such as Phe (trypanosomal form) or smaller residues such as Ser (human), resulted in slightly altered binding geometries, which may have played a role in determining the final product.[33] Interestingly, the serine and alanine mutants of Phe71 preserved the type III function of the native enzyme.

Table 1 shows that, like the WT TbPRMT7 system, the F71I mutant preferred to methylate the $N_{\eta 2}$ position with a computed $\Delta G^{\ddagger}$ of 18.3 ± 0.7 kcal/mol compared to 32.5 ± 1.5 kcal/mol for the $N_{\eta 1}$ position (Figure 8). The transition structures had similar $r(C_M–S_\delta)$ and $r(C_M–N_\eta)$ reacting distances of 2.2 Å for both binding orientations, i.e., MMA-$N_{\eta 1}$ and MMA-$N_{\eta 2}$ (Figure 9). Calculated CM3 charges[68] for the $N_{\eta 1}$ and $N_{\eta 2}$ atoms at the transition state found the reacting nitrogen be more negative for MMA-$N_{\eta 2}$, −0.83 e, relative to MMA-$N_{\eta 1}$, −0.73 e, which is indicative of an enhanced nucleophilicity for that particular orientation (Table 3). This may be the result of a shorter interacting distance (and presumably stronger hydrogen bond) between Gln329 and Arg during the transition state for MMA-$N_{\eta 2}$ with a Q329-O···$H_{\eta 11}$–$N_{\eta 1}$ length of 1.9 ± 0.2 Å compared to 2.7 ± 0.4 Å for MMA-$N_{\eta 1}$ (Figure 9). In addition, the Glu172 residue has the negatively charged carboxylate group positioned overall closer

DOI: 10.1021/acs.jcim.9b00137
J. Chem. Inf. Model. 2019, 59, 2913–2923

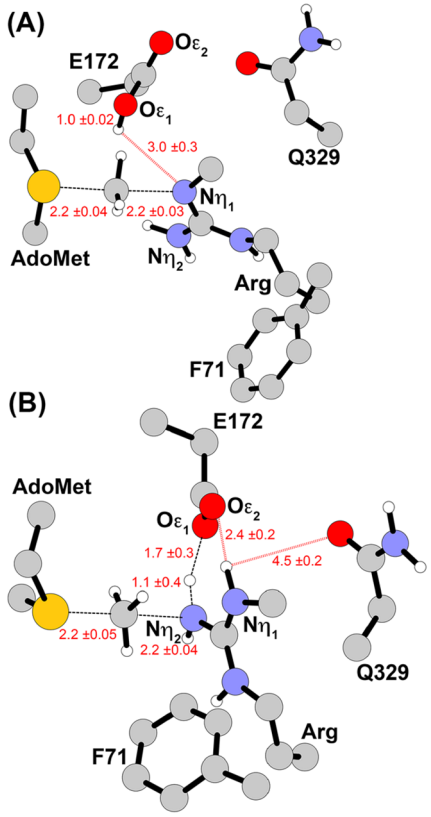

Figure 7. Active site structure from the QM/MM/MD transition state FEP window for the second methyl transfer from AdoMet to give (A) ADMA and (B) SDMA products for the MMA-$N_{\eta 1}$ peptide conformation in WT TbPRMT7. Distances are in angstroms.

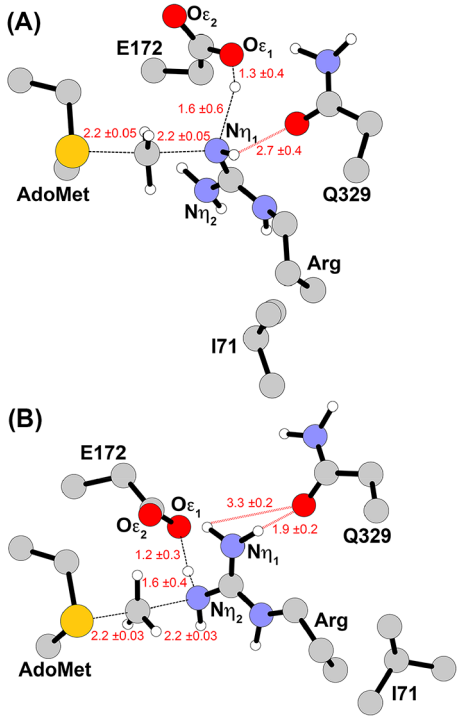

Figure 9. Active site structure from the QM/MM/MD transition state FEP window for the first methyl transfer from AdoMet to the (A) $N_{\eta 1}$ and (B) $N_{\eta 2}$ atoms of the arginine peptide in F71I TbPRMT7. Distances are in angstroms.

to the positively charged arginine guanidino group in the MMA-$N_{\eta 2}$ conformation (Supporting Information Figure S5).

Upon formation of monomethylated product (Supporting Information Figure S6), the MMA-$N_{\eta 2}$ binding orientation was also favored over the MMA-$N_{\eta 1}$ configuration with ΔG_{rxn} values of −16.0 ± 0.1 and −8.7 ± 1.7 kcal/mol, respectively (Table 1). Inspection of the binding geometry of the naked arginine transition state within the F71I TbPRMT7 active site (Supporting Information Figure S5) suggests a correlation between the ability of the active site residues Glu172 and Gln329 to electronically stabilize the substrate and the lowering of the activation barrier. However, unlike the WT TbPRMT7 the Glu172 residue in the F71I mutant was not as

Table 3. Average CM3 Charges for the $N_{\eta 1}$ and $N_{\eta 2}$ Atoms of Arginine in the Naked Peptide for the WT and F71I TbPRMT7 Enzymes during the Transition State to Form MMA Product

	WT MMA-$N_{\eta 1}$	WT MMA-$N_{\eta 2}$	F71I MMA-$N_{\eta 1}$	F71I MMA-$N_{\eta 2}$
$N_{\eta 1}$	−0.77	−0.62	−0.73	−0.62
$N_{\eta 2}$	−0.64	−0.78	−0.64	−0.83

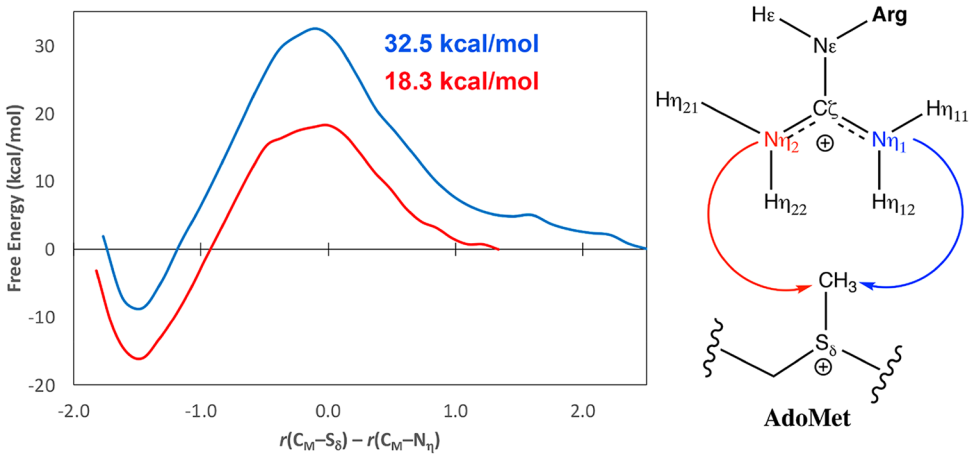

Figure 8. Free energy profiles and $\Delta G^{\ddagger}$ for the methyl transfer from AdoMet to the $N_{\eta 1}$ atom (blue) and $N_{\eta 2}$ atom (red) of the unmethylated arginine peptide in F71I TbPRMT7.

DOI: 10.1021/acs.jcim.9b00137
J. Chem. Inf. Model. 2019, 59, 2913−2923

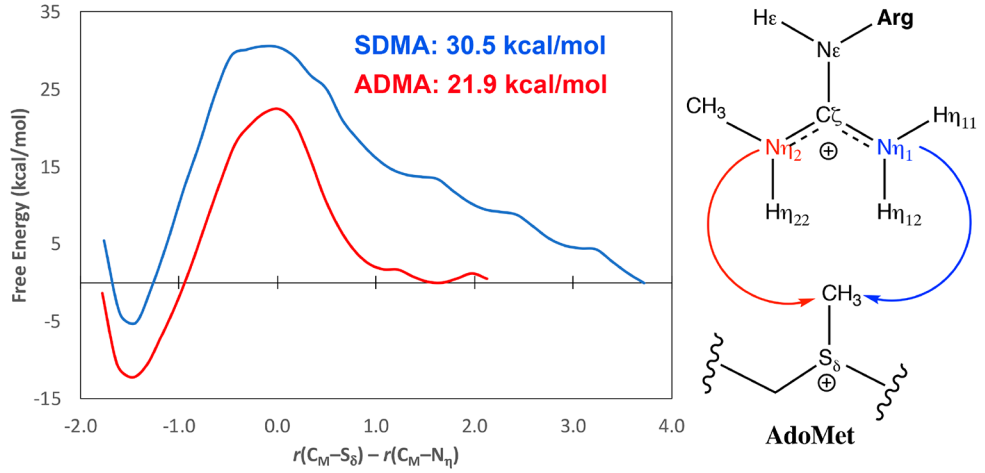

Figure 10. Free energy profiles and $\Delta G^{\ddagger}$ for the second methyl transfer from AdoMet to the $N_{\eta 1}$ atom (blue) and $N_{\eta 2}$ atom (red) of the monomethylated arginine peptide in F71I TbPRMT7.

ideally positioned within the active site to fully anchor the peptide substrate, e.g., the Glu172-$O_{\varepsilon 2}$ atom did not hydrogen bond with the proton on the opposite guanidino nitrogen atom (Figure 9 versus Figure 4). This may partially explain why $\Delta G^{\ddagger}$ increased to 18.3 ± 0.7 kcal/mol in the mutant compared to 16.9 ± 0.1 kcal/mol for WT (Table 1). The WT enzyme also had additional hydrogen bonding provided by Phe174 that was absent in the F71I mutant (Supporting Information Figure S2).

Following a processive mechanism, where the substrate is not released prior to the second methylation, the methyl transfer in F71I TbPRMT7 would again favor the MMA-$N_{\eta 2}$ orientation as the computed $\Delta G^{\ddagger}$ and ΔG_{rxn} values were both lower in energy than that of the MMA-$N_{\eta 1}$ configuration (Table 1). Interestingly, the second turnover yielded a reasonably low $\Delta G^{\ddagger}$ of 21.9 ± 0.7 kcal/mol for the ADMA-$N_{\eta 2}$ dimethylation product compared to a much larger $\Delta G^{\ddagger}$ of 30.5 ± 1.2 kcal/mol for the SDMA-$N_{\eta 2}$ product (Table 2 and Figure 10). With the isoleucine present in the active site, the MMA substrate was able to move deeper into the binding pocket where the $N_{\eta 2}$ of arginine could better interact with the base Glu172 (Supporting Information Figure S7). Favorable electrostatic interactions between the arginine substrate and the Glu172 and Gln329 residues were found again to be critical for orienting the peptide during the S_N2 mechanism. For example, Figure 11 highlights a close distance of 2.0 ± 0.2 Å between Q329-O···$H_{\eta 11}$–$N_{\eta 1}$ for the ADMA product route; however, the formation of SMDA increased the Q329-O···$H_{\eta 11}$–$N_{\eta 1}$ transition state distance to 4.2 ± 0.4 Å. The reduction of electronic stabilization from Gln329 upon the transition structure correlated with the increased activation barrier. In addition, generalized Born free energy decomposition calculations with AdoMet and MMA bound in the F71I TbPRMT7 active site found a large substrate ΔG_{bind} contribution from Gln329 for the ADMA-$N_{\eta 2}$ orientation with a value of −2.8 ± 0.7 kcal/mol compared to −0.02 ± 0.2 kcal/mol for SDMA-$N_{\eta 2}$ (Supporting Information Table S2).

The QM/MM/MD calculations agreed with our previous experiments showing the F71I TbPRMT7 mutant to be active with both a naked and monomethylated single-arginine peptide.[33] However, the experiment identified the presence of two dimethylated arginine species (ADMA and SDMA), whereas, the present simulations found the activation barrier

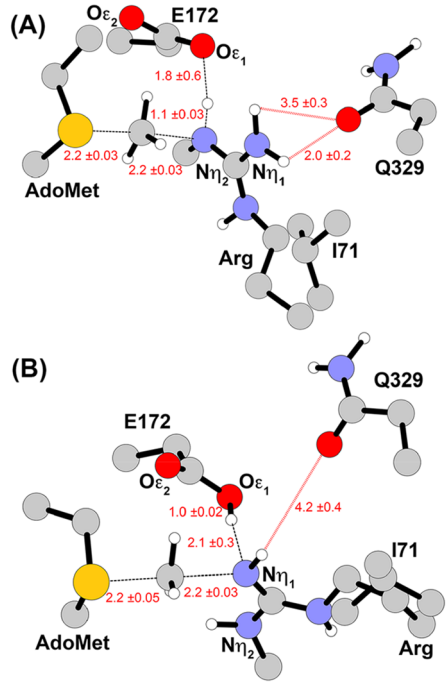

Figure 11. Active site structure from the QM/MM/MD transition state FEP window for the second methyl transfer from AdoMet to give (A) ADMA and (B) SDMA products for the MMA-$N_{\eta 1}$ peptide conformation in F71I TbPRMT7. Distances are in angstroms.

too large for SDMA formation. Despite considerable effort, a subsequent second turnover beginning from the MMA-$N_{\eta 1}$ orientation leading to either an ADMA-$N_{\eta 1}$ or SDMA-$N_{\eta 1}$ dimethylation product did not energetically converge in the simulations. This brings into question the viability of that binding configuration, particularly when considering the significantly higher ΔG_{rxn} of −8.7 ± 1.7 kcal/mol for binding in the MMA-$N_{\eta 1}$ orientation compared to −16.0 ± 0.1 kcal/mol for the MMA-$N_{\eta 2}$ configuration (Table 1 and Supporting Information Figure S6).

CONCLUSIONS

Mixed quantum mechanical and molecular mechanical simulations have been performed for wild-type and mutant

DOI: 10.1021/acs.jcim.9b00137
J. Chem. Inf. Model. 2019, 59, 2913−2923

TbPRMT7 enzymes to elucidate the role of electronics upon product specificity. Two structurally conserved glutamate residues from the "double-E" hairpin loop in WT TbPRMT7, i.e., Glu172 and Glu181, were explored as potential active site bases during the S_N2 mechanism. The QM/MM calculations coupled to molecular dynamics sampling and free energy perturbation theory found Glu172 to have a significantly lower $\Delta G^{\ddagger}$ compared to Glu181, i.e., 16.9 and 47.3 kcal/mol, respectively, when performing the proton transfer. Further scrutinization of the mechanism examined the ability of each guanidino nitrogen atom from the arginine substrate, $N_{\eta 1}$ and $N_{\eta 2}$, to function as the nucleophile during the first turnover to form the monomethylated product. The QM/MM/MD simulations predicted the $N_{\eta 2}$ atom to give lower $\Delta G^{\ddagger}$ and ΔG_{rxn} values for all WT and mutant enzymes, suggesting that the active site may be electrostatically preorganized to favor that particular reaction pathway. Detailed examination of the simulation trajectories found two WT TbPRMT7 active site residues, Glu172 and Gln329, to be particularly important for properly orienting the naked arginine peptide during the methylation reaction and for enhancing the nucleophilicity of the attacking guanidino group by reducing positive charge. Accentuating the importance of Gln329 was a computed increase in $\Delta G^{\ddagger}$ to 30.1 kcal/mol for the mutant Q329S TbPRMT7 compared to 16.9 kcal/mol for the WT enzyme. Fittingly, experimental mutations of Q329S and Q329H completely deleted or largely decreased the activity of TbPRMT7.[30]

The sequential transfer of methyl groups onto a single arginine peptide was examined using the QM/MM/MD calculations by following a processive manner, i.e., does not release the substrate prior to the second methylation, and a distributive manner, where the substrate is released after the first methylation. Following a processive mechanism,[66] the lowest energy reaction pathway computed for the second turnover led to the ADMA product with a large $\Delta G^{\ddagger}$ value of 28.8 kcal/mol. This substantial activation barrier would impede the formation of a dimethylated substrate as experimentally observed.[66] Interestingly, when following a distributive process, the formation of SDMA was predicted to be energetically feasible with a computed $\Delta G^{\ddagger}$ of 22.7 kcal/mol, whereas ADMA formation still gave a large $\Delta G^{\ddagger}$ of 29.9 kcal/mol. However, the formation of SDMA may be problematic as it would require the MMA substrate and AdoMet to both re-enter the enzyme through a narrow, sterically poor arginine binding pocket entrance and to rebind in an energetically poor conformation, i.e., MMA-$N_{\eta 1}$, prior to S_N2 attack.

The mutation of Phe71 to Ile has been shown to convert the enzyme from a type III PRMT into a mixed type I/II capable of forming three different arginine products (MMA, ADMA, and SDMA).[33] The calculations found that the F71I mutant energetically preferred to methylate the $N_{\eta 2}$ position on both the naked and monomethylated arginine substrates, which favorably correlated with a processive mechanism for PRMT7.[66] The second turnover was computed to yield a reasonable $\Delta G^{\ddagger}$ of 21.9 kcal/mol for the formation of ADMA-$N_{\eta 2}$, similar to the ADMA-producing Glu181Asp TbPRMT7 mutant.[31] While our previous experiments identified the presence of two dimethylated arginine species (ADMA and SDMA) for F71I TbPRMT7,[33] the present simulations found the activation barrier too large for SDMA formation at 30.5 kcal/mol. Electronic stabilization of the transition structure via Gln329 appears to make a major difference on the overall reaction energetics with a very large transition state distance between Gln329 and the Arg substrate of 4.2 Å for SDMA formation was compared to 2.0 Å for the energetically favored ADMA.

In summary, the present study found that Glu172 and Gln329 (TbPRMT7 numbering) in the WT and mutant TbPRMT7 enzymes may play major roles in product specificity by (1) properly orienting the peptide for S_N2 attack, (2) enhancing the nucleophilicity of the substrate guanidino group through the neutralization of positive charge, and (3) lowering the free energy of binding for the subsequent methylated products.

■ ASSOCIATED CONTENT

Supporting Information

The Supporting Information is available free of charge on the ACS Publications website at DOI: 10.1021/acs.jcim.9b00137.

Free energy decomposition energies for WT and F71I TbPRMT7; figures of mono- and dimethylated arginine substrate in the WT and F71I TbPRMT7 active sites from FEP windows at the transition state and products (PDF)

■ AUTHOR INFORMATION

Corresponding Author

*E-mail: orlando.acevedo@miami.edu.

ORCID

Joan M. Hevel: 0000-0002-9559-4635

Orlando Acevedo: 0000-0002-6110-3930

Notes

The authors declare no competing financial interest.

The authors will release the atomic coordinates upon article publication.

■ ACKNOWLEDGMENTS

Gratitude is expressed to the National Science Foundation (CHE-1626860 to O.A. and CHE-1412405 to J.M.H.) and the University of Miami Center for Computational Sciences for support of this research.

■ ABBREVIATIONS

PRMT7, protein arginine methyltransferase 7; MMA, monomethylarginine; ADMA, asymmetric dimethylarginine; SDMA, symmetric dimethylarginine; AdoMet, *S*-adenosyl-*L*-methionine; AdoHcy, *S*-adenosyl-*L*-homocysteine; QM/MM, quantum mechanics and molecular mechanics; MD, molecular dynamics

■ REFERENCES

(1) Biggar, K. K.; Li, S. S.-C. Non-Histone Protein Methylation as a Regulator of Cellular Signalling and Function. *Nat. Rev. Mol. Cell Biol.* **2015**, *16*, 5−17.

(2) Blanchet, F.; Cardona, A.; Letimier, F. A.; Hershfield, M. S.; Acuto, O. Cd28 Costimulatory Signal Induces Protein Arginine Methylation in T Cells. *J. Exp. Med.* **2005**, *202*, 371−377.

(3) Yadav, N.; Lee, J.; Kim, J.; Shen, J.; Hu, M. C.-T.; Aldaz, C. M.; Bedford, M. T. Specific Protein Methylation Defects and Gene Expression Perturbations in Coactivator-Associated Arginine Methyltransferase 1-Deficient Mice. *Proc. Natl. Acad. Sci. U. S. A.* **2003**, *100*, 6464−6468.

(4) Hang, R.; Liu, C.; Ahmad, A.; Zhang, Y.; Lu, F.; Cao, X. *Arabidopsis* Protein Arginine Methyltransferase 3 is Required for Ribosome Biogenesis by Affecting Precursor Ribosomal RNA Processing. *Proc. Natl. Acad. Sci. U. S. A.* **2014**, *111*, 16190−16195.
(5) Blanc, R. S.; Richard, S. Arginine Methylation: The Coming of Age. *Mol. Cell* **2017**, *65*, 8−24.
(6) Morales, Y.; Cáceres, T.; May, K.; Hevel, J. M. Biochemistry and Regulation of the Protein Arginine Methyltransferases (Prmts). *Arch. Biochem. Biophys.* **2016**, *590*, 138−152.
(7) Fuhrmann, J.; Clancy, K. W.; Thompson, P. R. Chemical Biology of Protein Arginine Modifications in Epigenetic Regulation. *Chem. Rev.* **2015**, *115*, 5413−5461.
(8) Pahlich, S.; Zakaryan, R. P.; Gehring, H. Protein Arginine Methylation: Cellular Functions and Methods of Analysis. *Biochim. Biophys. Acta, Proteins Proteomics* **2006**, *1764*, 1890−1903.
(9) Bedford, M. T.; Richard, S. Arginine Methylation an Emerging Regulator of Protein Function. *Mol. Cell* **2005**, *18*, 263−272.
(10) Wei, H.; Mundade, R.; Lange, K. C.; Lu, T. Protein Arginine Methylation of Non-Histone Proteins and its Role in Diseases. *Cell Cycle* **2014**, *13*, 32−41.
(11) Larsen, S. C.; Sylvestersen, K. B.; Mund, A.; Lyon, D.; Mullari, M.; Madsen, M. V.; Daniel, J. A.; Jensen, L. J.; Nielsen, M. L. Proteome-Wide Analysis of Arginine Monomethylation Reveals Widespread Occurrence in Human Cells. *Sci. Signaling* **2016**, *9*, rs9.
(12) Boffa, L. C.; Karn, J.; Vidali, G.; Allfrey, V. G. Distribution of Ng, Ng,-Dimethylarginine in Nuclear Protein Fractions. *Biochem. Biophys. Res. Commun.* **1977**, *74*, 969−976.
(13) Bedford, M. T.; Clarke, S. G. Protein Arginine Methylation in Mammals: Who, What, and Why. *Mol. Cell* **2009**, *33*, 1−13.
(14) Yang, Y.; Bedford, M. T. Protein Arginine Methyltransferases and Cancer. *Nat. Rev. Cancer* **2013**, *13*, 37−50.
(15) Tripsianes, K.; Madl, T.; Machyna, M.; Fessas, D.; Englbrecht, C.; Fischer, U.; Neugebauer, K. M.; Sattler, M. Structural Basis for Dimethylarginine Recognition by the Tudor Domains of Human Smn and Spf30 Proteins. *Nat. Struct. Mol. Biol.* **2011**, *18*, 1414−1420.
(16) Yang, Y.; Hadjikyriacou, A.; Xia, Z.; Gayatri, S.; Kim, D.; Zurita-Lopez, C.; Kelly, R.; Guo, A.; Li, W.; Clarke, S. G.; Bedford, M. T. Prmt9 is a Type II Methyltransferase that Methylates the Splicing Factor Sap145. *Nat. Commun.* **2015**, *6*, 6428.
(17) Feng, Y.; Maity, R.; Whitelegge, J. P.; Hadjikyriacou, A.; Li, Z.; Zurita-Lopez, C.; Al-Hadid, Q.; Clark, A. T.; Bedford, M. T.; Masson, J.-Y.; Clarke, S. G. Mammalian Protein Arginine Methyltransferase 7 (Prmt7) Specifically Targets RXR Sites in Lysine- and Arginine-Rich Regions. *J. Biol. Chem.* **2013**, *288*, 37010−37025.
(18) Gonsalvez, G. B.; Tian, L.; Ospina, J. K.; Boisvert, F.-M.; Lamond, A. I.; Matera, A. G. Two Distinct Arginine Methyltransferases are Required for Biogenesis of Sm-Class Ribonucleoproteins. *J. Cell Biol.* **2007**, *178*, 733−740.
(19) Karkhanis, V.; Wang, L.; Tae, S.; Hu, Y.-J.; Imbalzano, A. N.; Sif, S. Protein Arginine Methyltransferase 7 Regulates Cellular Response to DNA Damage by Methylating Promoter Histones H2a and H4 of the Polymerase Δ Catalytic Subunit Gene, Pold1. *J. Biol. Chem.* **2012**, *287*, 29801−29814.
(20) Geng, P.; Zhang, Y.; Liu, X.; Zhang, N.; Liu, Y.; Liu, X.; Lin, C.; Yan, X.; Li, Z.; Wang, G.; Li, Y.; Tan, J.; Liu, D.-X.; Huang, B.; Lu, J. Automethylation of Protein Arginine Methyltransferase 7 and its Impact on Breast Cancer Progression. *FASEB J.* **2017**, *31*, 2287−2300.
(21) Yao, R.; Jiang, H.; Ma, Y.; Wang, L.; Wang, L.; Du, J.; Hou, P.; Gao, Y.; Zhao, L.; Wang, G.; Zhang, Y.; Liu, D.-X.; Huang, B.; Lu, J. Prmt7 Induces Epithelial-to-Mesenchymal Transition and Promotes Metastasis in Breast Cancer. *Cancer Res.* **2014**, *74*, 5656−5667.
(22) Jeong, H.-J.; Lee, H.-J.; Vuong, T. A.; Choi, K.-S.; Choi, D.; Koo, S.-H.; Cho, S. C.; Cho, H.; Kang, J.-S. Prmt7 Deficiency Causes Reduced Skeletal Muscle Oxidative Metabolism and Age-Related Obesity. *Diabetes* **2016**, *65*, 1868−1882.
(23) Agolini, E.; Dentici, M. L.; Bellacchio, E.; Alesi, V.; Radio, F. C.; Torella, A.; Musacchia, F.; Tartaglia, M.; Dallapiccola, B.; Nigro, V.; Digilio, M. C.; Novelli, A. Expanding the Clinical and Molecular Spectrum of Prmt7Mutations: Three Additional Patients and Review. *Clin. Genet.* **2018**, *93*, 675−681.
(24) Migliori, V.; Müller, J.; Phalke, S.; Low, D.; Bezzi, M.; Mok, W. C.; Sahu, S. K.; Gunaratne, J.; Capasso, P.; Bassi, C.; Cecatiello, V.; Marco, A. D.; Blackstock, W.; Kuznetsov, V.; Amati, B.; Mapelli, M.; Guccione, E. Symmetric Dimethylation of H3r2 is a Newly Identified Histone Mark that Supports Euchromatin Maintenance. *Nat. Struct. Mol. Biol.* **2012**, *19*, 136−144.
(25) Miranda, T. B.; Miranda, M.; Frankel, A.; Clarke, S. Prmt7 is a Member of the Protein Arginine Methyltransferase Family with a Distinct Substrate Specificity. *J. Biol. Chem.* **2004**, *279*, 22902−22907.
(26) Lee, J.-H.; Cook, J. R.; Yang, Z.-H.; Mirochnitchenko, O.; Gunderson, S. I.; Felix, A. M.; Herth, N.; Hoffmann, R.; Pestka, S. Prmt7, a New Protein Arginine Methyltransferase that Synthesizes Symmetric Dimethylarginine. *J. Biol. Chem.* **2005**, *280*, 3656−3664.
(27) Zurita-Lopez, C. I.; Sandberg, T.; Kelly, R.; Clarke, S. G. Human Protein Arginine Methyltransferase 7 (Prmt7) Is a Type III Enzyme Forming W-Ng-Monomethylated Arginine Residues. *J. Biol. Chem.* **2012**, *287*, 7859−7870.
(28) Fisk, J. C.; Sayegh, J.; Zurita-Lopez, C.; Menon, S.; Presnyak, V.; Clarke, S. G.; Read, L. K. A Type III Protein Arginine Methyltransferase from the Protozoan Parasite Trypanosoma Brucei. *J. Biol. Chem.* **2009**, *284*, 11590−11600.
(29) Feng, Y.; Hadjikyriacou, A.; Clarke, S. G. Substrate Specificity of Human Protein Arginine Methyltransferase 7 (Prmt7). *J. Biol. Chem.* **2014**, *289*, 32604−32616.
(30) Wang, C.; Zhu, Y.; Caceres, T. B.; Liu, L.; Peng, J.; Wang, J.; Chen, J.; Chen, X.; Zhang, Z.; Zuo, X.; Gong, Q.; Teng, M.; Hevel, J. M.; Wu, J.; Shi, Y. Structural Determinants for the Strict Monomethylation Activity by Trypanosoma Brucei Protein Arginine Methyltransferase 7. *Structure* **2014**, *22*, 756−768.
(31) Debler, E. W.; Jain, K.; Warmack, R. A.; Feng, Y.; Clarke, S. G.; Blobel, G.; Stavropoulos, P. A Glutamate/Aspartate Switch Controls Product Specificity in a Protein Arginine Methyltransferase. *Proc. Natl. Acad. Sci. U. S. A.* **2016**, *113*, 2068.
(32) Jain, K.; Warmack, R. A.; Debler, E. W.; Hadjikyriacou, A.; Stavropoulos, P.; Clarke, S. G. Protein Arginine Methyltransferase Product Specificity Is Mediated by Distinct Active-Site Architectures. *J. Biol. Chem.* **2016**, *291*, 18299−18308.
(33) Caceres, T.; Thakur, A.; Price, O. M.; Ippolito, N.; Li, J.; Qu, J.; Acevedo, O.; Hevel, J. M. Phe 71 in Type III Trypanosomal Protein Arginine Methyltransferase 7 (Tbprmt7) Restricts the Enzyme to Monomethylation. *Biochemistry* **2018**, *57*, 1349−1359.
(34) Krieger, E.; Vriend, G. Yasara View - Molecular Graphics for All Devices - from Smartphones to Workstations. *Bioinformatics* **2014**, *30*, 2981−2982.
(35) Case, D. A.; Cheatham, T. E., 3rd; Darden, T.; Gohlke, H.; Luo, R.; Merz, K. M., Jr.; Onufriev, A.; Simmerling, C.; Wang, B.; Woods, R. J. The ABMER Biomolecular Simulation Programs. *J. Comput. Chem.* **2005**, *26*, 1668−1688.
(36) Jorgensen, W. L.; Chandrasekhar, J.; Madura, J. D.; Impey, R. W.; Klein, M. L. Comparison of Simple Potential Functions for Simulating Liquid Water. *J. Chem. Phys.* **1983**, *79*, 926−935.
(37) Maier, J. A.; Martinez, C.; Kasavajhala, K.; Wickstrom, L.; Hauser, K. E.; Simmerling, C. FF14sb: Improving the Accuracy of Protein Side Chain and Backbone Parameters from FF99sb. *J. Chem. Theory Comput.* **2015**, *11*, 3696−3713.
(38) Wang, J.; Wolf, R. M.; Caldwell, J. W.; Kollman, P. A.; Case, D. A. Development and Testing of a General AMBER Force Field. *J. Comput. Chem.* **2004**, *25*, 1157−1174.
(39) Salomon-Ferrer, R.; Gotz, A. W.; Poole, D.; Le Grand, S.; Walker, R. C. Routine Microsecond Molecular Dynamics Simulations with AMBER on GPUs. 2. Explicit Solvent Particle Mesh Ewald. *J. Chem. Theory Comput.* **2013**, *9*, 3878−3888.
(40) Acevedo, O.; Jorgensen, W. L. Advances in Quantum and Molecular Mechanical (QM/MM) Simulations for Organic and Enzymatic Reactions. *Acc. Chem. Res.* **2010**, *43*, 142−151.
(41) Acevedo, O.; Jorgensen, W. L. Quantum and Molecular Mechanical (QM/MM) Monte Carlo Techniques for Modeling

DOI: 10.1021/acs.jcim.9b00137
J. Chem. Inf. Model. 2019, 59, 2913−2923

Condensed-Phase Reactions. *WIREs Comput. Mol. Sci.* **2014**, *4*, 422−435.
(42) Elstner, M. The SCC-DFTB Method and its Application to Biological Systems. *Theor. Chem. Acc.* **2006**, *116*, 316−325.
(43) Seabra, G. d. M.; Walker, R. C.; Elstner, M.; Case, D. A.; Roitberg, A. E. Implementation of the SCC-DFTB Method for Hybrid QM/MM Simulations within the AMBER Molecular Dynamics Package. *J. Phys. Chem. A* **2007**, *111*, 5655−5664.
(44) Aradi, B.; Hourahine, B.; Frauenheim, T. Dftb+, a Sparse Matrix-Based Implementation of the Dftb Method. *J. Phys. Chem. A* **2007**, *111*, 5678−5684.
(45) Chu, Y.; Li, G.; Guo, H. QM/MM MD and Free Energy Simulations of the Methylation Reactions Catalyzed by Protein Arginine Methyltransferase Prmt3. *Can. J. Chem.* **2013**, *91*, 605−612.
(46) Repasky, M. P.; Chandrasekhar, J.; Jorgensen, W. L. PDDG/PM3 and PDDG/MNDO: Improved Semiempirical Methods. *J. Comput. Chem.* **2002**, *23*, 1601−1622.
(47) Christensen, A. S.; Kubař, T.; Cui, Q.; Elstner, M. Semiempirical Quantum Mechanical Methods for Noncovalent Interactions for Chemical and Biochemical Applications. *Chem. Rev.* **2016**, *116*, 5301−5337.
(48) Cui, Q. Perspective: Quantum Mechanical Methods in Biochemistry and Biophysics. *J. Chem. Phys.* **2016**, *145*, 140901.
(49) van der Kamp, M. W.; Mulholland, A. J. Combined Quantum Mechanics/Molecular Mechanics (QM/MM) Methods in Computational Enzymology. *Biochemistry* **2013**, *52*, 2708−2728.
(50) Walker, R. C.; Crowley, M. F.; Case, D. A. The Implementation of a Fast and Accurate QM/MM Potential Method in AMBER. *J. Comput. Chem.* **2008**, *29*, 1019−1031.
(51) Kästner, J. Umbrella Sampling. *WIREs Comput. Mol. Sci.* **2011**, *1*, 932−942.
(52) Kumar, S.; Rosenberg, J. M.; Bouzida, D.; Swendsen, R. H.; Kollman, P. A. The Weighted Histogram Analysis Method for Free-Energy Calculations on Biomolecules. I. The Method. *J. Comput. Chem.* **1992**, *13*, 1011−1021.
(53) Vilseck, J. Z.; Acevedo, O. Computing Free-Energy Profiles using Multidimensional Potentials of Mean Force and Polynomial Quadrature Methods. *Annu. Rep. Comput. Chem.* **2010**, *6*, 37−49.
(54) Callegari, D.; Ranaghan, K. E.; Woods, C. J.; Minari, R.; Tiseo, M.; Mor, M.; Mulholland, A. J.; Lodola, A. L718q Mutant Egfr Escapes Covalent Inhibition by Stabilizing a Non-Reactive Conformation of the Lung Cancer Drug Osimertinib. *Chem. Sci.* **2018**, *9*, 2740−2749.
(55) Capoferri, L.; Lodola, A.; Rivara, S.; Mor, M. Quantum Mechanics/Molecular Mechanics Modeling of Covalent Addition between Egfr−Cysteine 797 and N-(4-Anilinoquinazolin-6-Yl) Acrylamide. *J. Chem. Inf. Model.* **2015**, *55*, 589−599.
(56) Cheng, X.; Collins, R. E.; Zhang, X. Structural and Sequence Motifs of Protein (Histone) Methylation Enzymes. *Annu. Rev. Biophys. Biomol. Struct.* **2005**, *34*, 267−294.
(57) Yue, Y.; Chu, Y.; Guo, H. Computational Study of Symmetric Methylation on Histone Arginine Catalyzed by Protein Arginine Methyltransferase Prmt5 through QM/MM MD and Free Energy Simulations. *Molecules* **2015**, *20*, 10032−10046.
(58) Gohlke, H.; Kiel, C.; Case, D. A. Insights into Protein−Protein Binding by Binding Free Energy Calculation and Free Energy Decomposition for the Ras−Raf and Ras−Ralgds Complexes. *J. Mol. Biol.* **2003**, *330*, 891−913.
(59) Brown, J. I.; Koopmans, T.; Strien, J. v.; Martin, N. I.; Frankel, A. Kinetic Analysis of Prmt1 Reveals Multifactorial Processivity and a Sequential Ordered Mechanism. *ChemBioChem* **2018**, *19*, 85−99.
(60) Gui, S.; Wooderchak-Donahue, W. L.; Zang, T.; Chen, D.; Daly, M. P.; Zhou, Z. S.; Hevel, J. M. Substrate-Induced Control of Product Formation by Protein Arginine Methyltransferase 1. *Biochemistry* **2013**, *52*, 199−209.
(61) Wang, M.; Xu, R.-M.; Thompson, P. R. Substrate Specificity, Processivity, and Kinetic Mechanism of Protein Arginine Methyltransferase 5. *Biochemistry* **2013**, *52*, 5430−5440.
(62) Obianyo, O.; Osborne, T. C.; Thompson, P. R. Kinetic Mechanism of Protein Arginine Methyltransferase. *Biochemistry* **2008**, *47*, 10420−10427.
(63) Lakowski, T. M.; Frankel, A. A Kinetic Study of Human Protein Arginine N-Methyltransferase 6 Reveals a Distributive Mechanism. *J. Biol. Chem.* **2008**, *283*, 10015−10025.
(64) Kölbel, K.; Ihling, C.; Bellmann-Sickert, K.; Neundorf, I.; Beck-Sickinger, A. G.; Sinz, A.; Kühn, U.; Wahle, E. Type I Arginine Methyltransferases Prmt1 and Prmt-3 Act Distributively. *J. Biol. Chem.* **2009**, *284*, 8274−8282.
(65) Hu, H.; Luo, C.; Zheng, Y. G. Transient Kinetics Define a Complete Kinetic Model for Protein Arginine Methyltransferase 1. *J. Biol. Chem.* **2016**, *291*, 26722−26738.
(66) Hasegawa, M.; Toma-Fukai, S.; Kim, J.-D.; Fukamizu, A.; Shimizu, T. Protein Arginine Methyltransferase 7 Has a Novel Homodimer-Likestructure Formed by Tandem Repeats. *FEBS Lett.* **2014**, *588*, 1942−1948.
(67) Durrant, J. D.; de Oliveira, C. A.; McCammon, J. A. POVME: An Algorithm for Measuring Binding-Pocket Volumes. *J. Mol. Graphics Modell.* **2011**, *29*, 773−776.
(68) Thompson, J. D.; Cramer, C. J.; Truhlar, D. G. Parameterization of Charge Model 3 for AM1, PM3, BLYP, and B3LYP. *J. Comput. Chem.* **2003**, *24*, 1291−1304.

DOI: 10.1021/acs.jcim.9b00137
J. Chem. Inf. Model. 2019, 59, 2913−2923